Ultrafast photoinduced insulator-to-metal transitions in vanadium dioxide

Michel van Veenendaal

Phys. Rev. B **87**, 235118 — Published 14 June 2013

DOI: 10.1103/PhysRevB.87.235118

Ultrafast Photoinduced Insulator-to-Metal Transitions in Vanadium Dioxide

Michel van Veenendaal
Dept. of Physics, Northern Illinois University, De Kalb, Illinois 60115
Advanced Photon Source, Argonne National Laboratory,
9700 South Cass Avenue, Argonne, Illinois 60439
(Dated: May 31, 2013)

An explanation is given for the ultrafast insulator-to-metal transition in VO_2 following photoexcitation. The photoinduced orbital imbalance induces a coherent motion of the V-V dimers affecting the electronic structure. After the closing of the gap, Boltzmann scattering equilibrates the electron densities. If the electron density exceeds a critical value, a phase transition occurs to the metallic state. The model explains several key features, such as a structural bottleneck, coherent structural motion combined with phase shifts in the oscillation, the absence of ultrafast metal-to-insulator transitions, and the need for a critical fluency.

PACS numbers: 71.30.+h, 78.47.jh, 78.47.J-

I. INTRODUCTION

The last decade has shown tremendous experimental progress in the study of the ultrafast response of materials to optical pulses in the sub-100-fs range. Nonequilibrium dynamics following the photoexcitation can lead to surprisingly fast transitions between competing phases leading to, for example, quenching of the magnetic order[1], insulator-to-metal transitions[2–16], unexpected phases[17,18], and melting of charge-density waves or stripes[19–21]. The theoretical understanding of these fascinating effects has not kept pace with the experimental advances and is often limited to phenemenological Landau-type models[20], exact diagonalizations of small systems[22,23] or three-temperature models[1,11,21]. For insulator-to-metal transitions in transition-metal oxides in particular, effects have only been described at a qualititative level due to the complex interplay between the structural, charge, orbital, and spin degrees of freedom.

The physics underlying insulator-metal transitions is one of the most intriguing questions in materials science. Ultrafast science allows the study of the physical pathways between the different structural and electronic phases and the competition between the various interactions. A prototypical example is vanadium dioxide, a compound that has been studied extensively. The $3d^1$ compound VO_2 undergoes a transition from a high-temperature metallic rutile phase to a low-temperature insulating monoclinic phase. The qualitative aspects of the phase transition are well known[27]. The octahedral oxygen surrounding causes the d orbital to split into threefold- t_{2g} and twofold-degenerate e_g multiplets. The VO_6 octahedra form edge-sharing chains, further lowering the symmetry splitting the t_{2g} states into an a_{1g} orbital ($d_\parallel$) and two e_g^π orbitals (d_π). In the metallic state, all t_{2g} orbitals are occupied with a somewhat larger electron density in the d_π band. In the monoclinic structure, the chains dimerize and the resulting V-V pairs twist. This creates bonding and antibonding $d_\parallel$ bands. The number of electrons in the d_π strongly is strongly reduced leading to a filled bonding $d_\parallel$ band. Although this molecular-orbital picture seems reasonable, theoretical approaches based on Density Functional Theory are not capable of describing the insulating behavior and electron-electron interactions need to be included[28].

In ultrafast spectroscopy, VO_2 has been one of the most studied systems[2–11]. Insulator-to-metal transitions in VO_2 have been induced using fields in the optical[2–10], terahertz[11], and X-ray region[13]. It has been established that structural changes play an essential role in the transition[2,3]. Cavalleri *et al.*[3] demonstrated the presence of an 80-fs delay between the photoinjection of electron-hole pairs and the change in reflectivity. They ascribed this delay to coherent structural motion. This was confirmed by Kübler *et al.*[6,7] who observed a 6-THz coherent modulation in the optical conductivity lasting for approximately 1 ps, which they interpreted as a wave packet motion of the V-V dimers. In addition, dynamical changes in orbital occupancies were observed using femtosecond X-ray absorption spectroscopy[4]. Cocker *et al.*[10] established a phase diagram of critical pump fluency versus temperature and show that a critical density of excited electrons and phonons is necessary to induce a phase transition. The critical fluency is reduced when approaching the critical temperature due to a decrease in tilting angle[8]. The ultrafast switching of the optical and electrical properties have inspired a wide range of possible applications[26].

II. MODEL

This paper focuses on the physical mechanism underlying the 100-fs insulator-to-metal transition by an ultrashort optical pulse. The model provides an intuitive explanation for the transition and in addition explains the experimentally observed effects. The description of the ultrafast insulator-to-metal transitions requires the inclusion of several components: optical excitation, electron-electron scattering to establish a thermal equilibrium, the coherent motion of the V-V dimers and the accompany-

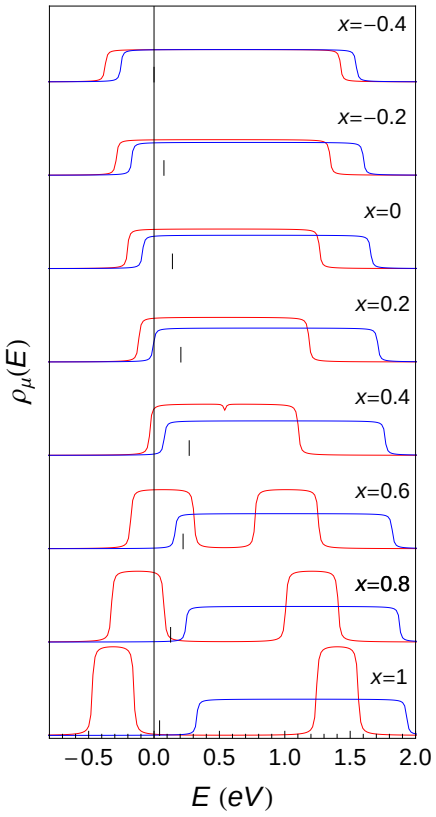

FIG. 1: Dependence of the densities of states $\rho_\mu(E)$ for $\mu = d_\parallel$ (red), d_π (blue) for different values of the generalized coordinate x. The small vertical lines denote the positions of the Fermi level.

ing changes in electronic structure. Although separately these aspects can be described in much greater detail, an integrated description of femtosecond dynamics requires some approximations.

Let us first discuss the electronic structure. Despite disagreement over the details of the band structure and the nature of the gap[27,28], there appears to be a general consensus that in the metallic state the Fermi lies in both d_π and $d_\parallel$ bands. The dimerization and tilting of the vanadium pairs then leads to the insulating state characterized by the formation of bonding and antibonding $d_\parallel$ bands. The conduction and valence bands closest to the Fermi level are the d_π and the bonding $d_\parallel$ bands, respectively. We assume that the electronic structure can be described by an effective Goodenough-model[27] using gaussian-broadened square densities of states. The insulator-to-metal transition is directly related to the coherent dimerization and tilting of the vanadium dimers. Since no detailed *ab initio* calculations of the changes in the density of states due to the coherent motion of the V-V dimers exist, they are modeled using a single effective dimensionless coordinate x. The change in densities of states $\rho_\mu(x, E)$ with $\mu = d_\parallel, d_\pi$ are taken linear with x. The model densities of states for different values of x are given in Fig. 1. In the insulating state ($x = 1.0$), the dimerization splits the $d_\parallel$ band into bonding and antibonding bands separated by about 1.9 eV; the insulating gap between the $d_\parallel$ and d_π bands is 0.5 eV.[28] The Fermi level lies inside the gap, so that the bonding $d_\parallel$ is filled. In the metallic state ($x = -0.4$), the Fermi level lies inside the $d_\parallel$ and d_π bands giving, following Biermann *et al.*[28], occupations of 0.42 and 0.58, respectively. The bandwidths are around 2 eV. As x changes from 1 to -0.4, there is a decrease in the dimerization of the $d_\parallel$ band and an increase in width of both bands. An important point is the value for which the gap closes, which is taken at $x = 0.4$. For $x = 1$ to 0.4, the electronic energy increases due to the decrease in dimerization which stabilizes the insulating state. From $x = 0.4$ to $x = -0.4$, the energy decreases again due to the increase in band width which stabilizes the metallic state.

The energy related to the structural distortion of the system is expressed in terms of the generalized coordinate x as

$$\varepsilon(x) \;=\; \alpha x^2 - \beta x(n_\parallel - n_\pi) \qquad (1)$$

containing a quadratic harmonic part and a linear term describing the interaction between the lattice and the electron densities in the $d_\parallel$ and d_π orbitals. The constant for the harmonic part $\alpha = 0.65$ eV. Viewing the problem in terms of a displaced harmonic oscillator, this coefficient corresponds to $\alpha = \frac{1}{2}M_{\rm eff}\omega^2X^2$, where $M_{\rm eff}$ is the effective mass of the atoms involved in the 6 Thz dimerization and tilting. The factor X describes the relation between the effective dimensionless coordinate x and the displacement xX. When the effective mass is equal to two edge-sharing VO_6 clusters, $X = 0.19$ Å. For the term linear in the displacement, we take $\beta = 0.42$ eV. This term corresponds to $\beta = M_{\rm eff}\omega^2X^2x_0$, where $x_0 = 0.37$. The energy gain from the displacement is then $-\frac{1}{2}M_{\rm eff}X^2x_0^2 = -0.32$ eV. This energy gain resulting from the electron-phonon coupling helps to stabilize the insulating state. The total energy at a particular time t is given by

$$E_{\rm tot}(t,x) \;=\; \sum_{\mu=d_\parallel,d_\pi} \int dE\ \rho_\mu(x(t),E) f_\mu^+(t,E)E + \varepsilon(x(t)),$$

where $f_\mu^+(t,E)$ are the electron occupations for the $\mu = d_\parallel, d_\pi$ orbitals. The total energy for 110-K Fermi-Dirac distribution functions is given by the thick-dashed grey line in Fig. 2. The minima for the metallic and insulating state when $f_\mu^+(t,E)$ are Fermi-Dirac distributions lie around $x = -0.36$ and 1.05, respectively. This gives a change in x of $\Delta x = 1.41$ leading to an effective displacement of $\Delta xX = 1.41X = 0.26$ Å. The maximum in energy occurs around $x = 0.4$ when the gap in the $d_\parallel$ band closes.

Electron-hole pairs are excited starting from a Fermi-Dirac occupation 110 K using an exponential probability $\exp[-(E - \hbar\omega_{\rm opt})^2/W^2]$, where the center of the excitation is $\hbar\omega_{\rm opt} = 1.5$ eV and the width is $W = 0.5$ eV. For each time step, the variation of $E_{\rm tot}(x)$ is calculated

around the current position. The coordinate describes a damped oscillatory motion in the dynamic potential landscape with a frequency given by $\omega\sqrt{1-\zeta^2}$ where $\omega/2\pi = 6$ THz and $\zeta = 0.1$. The damping is given by $e^{-\zeta\omega t}$. For the 6 THz oscillation, this gives a damping time of 1.66 ps. The structural motion causes dynamic changes in the density of states. We assume that the occupations $f_\mu(t,E)$ follow the changes in $\rho_\mu(x,E)$ adiabatically. Furthermore, at each time step, the occupations are adjusted using Boltzmann equations[29]. The scattering can change the occupation at energy E in the band with index μ by

$$\frac{\partial f_\mu(t,E)}{\partial t} = F_\mu^+(t,E) - F_\mu^-(t,E). \quad (2)$$

The collision terms due to the electron-electron scattering are given by

$$F_\mu^\pm(t,E) = \frac{2\pi}{\hbar}\sum_{\mu'}\int d\epsilon\; m_{\mu\mu'} w(\epsilon)\rho_{\mu'}(x(t),E\mp\epsilon) \times f_{\mu'}^\pm(t,E\mp\epsilon) f_\mu^\mp(t,E), \quad (3)$$

where $f_{\mu'}^+(t,E\mp\epsilon)$ is the electron distribution function for the orbital μ at time t; the hole occupation is $f_{\mu'}^-(t,E) = 1 - f_{\mu'}^+(t,E)$. The function $w(\epsilon)$ is given by

$$w(\epsilon) = \sum_{\mu\mu'}\int dE\; m_{\mu\mu'}\rho_{\mu'}(x(t),E-\epsilon)\rho_\mu(x(t),E) \times f_{\mu'}^-(t,E-\epsilon) f_\mu^+(t,E) \quad (4)$$

gives the scattering strength for an energy ϵ. The matrix element $m_{\mu\mu'} = 6$ eV. Cooling of the excited electron-hole pairs is included via coupling to a phonon bath at a temperature of 110 K. The maximum phonon energy is 75 meV. The cooling due to phonon scattering occurs on a timescale larger than the insulator-to-metal transition.

It is important to realize that the double potential well as a function of the effective displacement x only occurs when the electron occupations are given by the Fermi-Dirac distribution and therefore involves changing the occupations of the d_π and $d_\parallel$ states as a function of x. When the energy is calculated without electron scattering, no double-well potential is obtained. With electron occupations n_π =0.58 and $n_\parallel = 1 - n_\pi$ =0.42, there is only a single minimum around $x = -0.36$, i.e. the value of x in the metallic state (this situation is approximately described by the thick red line in Fig. 2). For densities that are found in the insulating state ($n_\pi = 0$), the minimum is around x =1.05. There is a second minimum, but that is now significantly higher in energy. This clearly demonstrates the importance of electron scattering between the d_π and $d_\parallel$ bands during the coherent motion.

III. RESULTS

Let us now look at the behavior of the electronic structure after photoexcitation in the insulating state. We take the photoexcitation as an instantaneous injection of electrons over the insulating gap into the d_π and antibonding $d_\parallel$ bands with an average excitation energy of 1.5 eV. The density of states $\rho_\mu(E)$, the electron occupation $f_\mu(E)$, and the electron density $n_\mu(E) = \rho_\mu(E) f_\mu(E)$ for $\mu = d_\parallel$ and d_π just after the photoexcitation are given in Fig. 3 for $t = 0$. For the optically-induced insulator-to-metal transition, the detailed nature of the excitation is often less relevant, since any "prepared" state created by the photoexcitation is removed by the electron-electron scattering in the first tens of femtoseconds, see the results for $t = 2, 8, 32$, and 48 fs in Fig. 3. The electron distribution function quickly develops towards a Fermi-Dirac distribution at elevated temperatures. Note that some anomalous behavior occurs in the the occupation functions $f_\mu(E)$ in regions where the density of states $\rho_\mu(E)$ is very small. However, this anomalous behavior does not affect the electron densities $n_\mu(E)$.

The photoinjection creates a finite electron density in

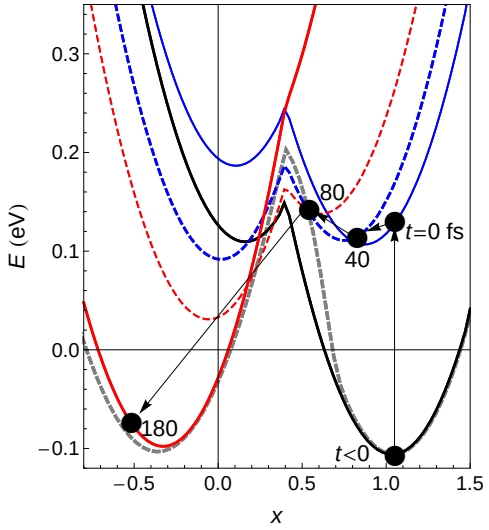

FIG. 2: The change in potential landscape for the coherent motion as a function of time t. The dashed-grey double potential well shows the total electronic and potential energy E as a function of the generalized dimensionless coordinate x that describes the dimerization and tilting of the vanadium pairs. The occupations are given by a 110-Kelvin Fermi-Dirac distribution. In the metallic state ($x = -0.36$), the electron densities are n_π =0.58 and $n_\parallel = 1 - n_\pi$ =0.42; in the insulating state (x =1.05), $n_\pi = 0$. The other energy curves are calculated at different times t relative to the photoexcitation. The electron densities are kept fixed as a function of x and the excited occupations are changed adiabatically with the densities of states. The black dots indicate the actual value of the coordinate x at that time. The black line shows the energy E before the excitation ($t < 0$) with n_π kept at zero for all x. The solid blue line ($t = 0$) shows the change in the energy dependence as a result of the photoinduced electron-hole pairs across the insulating gap leading to $n_\pi = 0.086$. The dashed blue, dashed-red, and red lines show the constant-density energy curves at $t = 40$, 80, and 180 fs with n_π=0.16, 0.24, and 0.56, respectively.

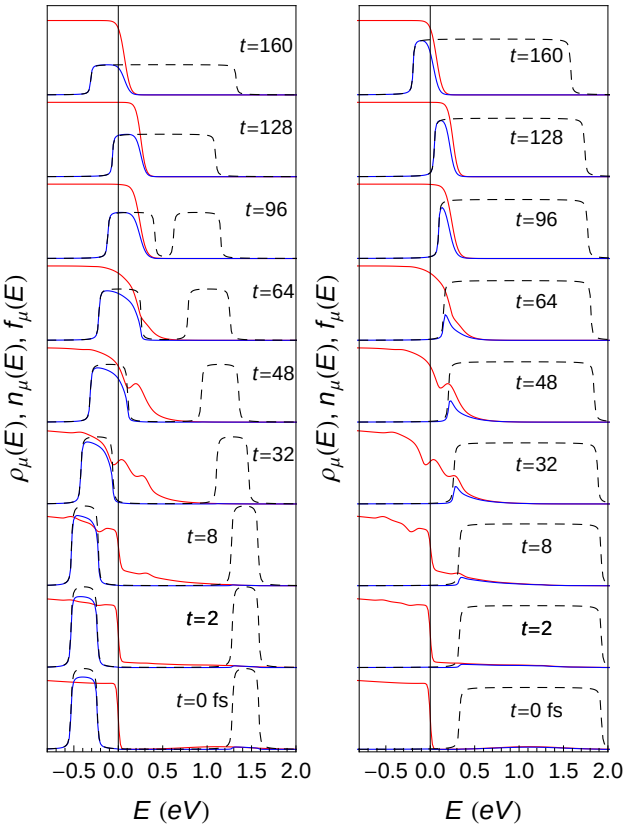

FIG. 3: The density of states $\rho_\mu(E)$ (dashed-grey), the electron occupation $f_\mu(E) = f^+_\mu(E)$ (red), and the electron density $n_\mu(E) = \rho_\mu(E) f_\mu(E)$ (blue) for $\mu = d_\parallel$ (left) and d_π (right) at selected times t after the photoexcitation.

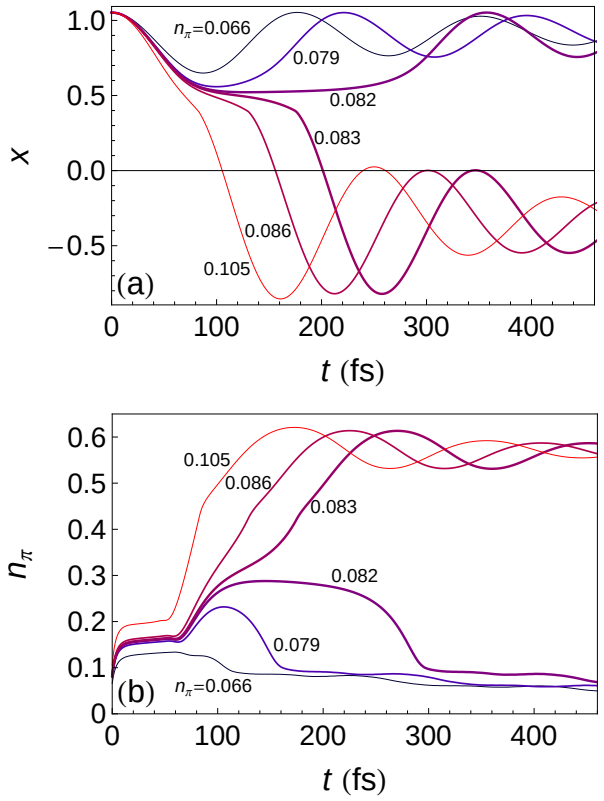

FIG. 4: The effective dimerization coordinate x and the density n_π in the in the d_π orbital as a function of time t. (a), The effective coordinate x describes the dimerization and tilting of the vanadium pairs in VO_2. The values of x as a function of time t are shown for different initial photoexcited densities in the d_π orbital with n_π =0.066, 0.076, 0.082, 0.083, 0.086 and 0.105. The values n_π =0.082 and 0.083 are just below and above the critical photoinjection density. (b) the same but for the density n_π.

the π orbital. Figure 4 shows the behavior of n_π and x for several photoinduced values of n_π as a function of time after the initial photoexcitation. In the first 20 fs, there is an additional increase in n_π, due to the relaxation of the photoexcited electrons from the antibonding $d_\parallel$ band due to the electron-electron scattering. The relaxation can be more clearly observed when we look at the total electron density $n(E) = \sum_\mu n_\mu(E)$ as a function of energy and time, see Fig. 5. The decrease in electron density in the antibonding π states is observed from 1.3 eV and up in the first 20 fs. The initial change in electron density is relatively small and the values of n_π and $n_\parallel$ are still significantly different from those in the metallic state. Furthermore, although the increase in n_π has affected the potential as a function of x, see the solid blue line in Fig. 2, the minimum of the metallic potential well is still significantly higher indicating that a significant change in electron densities is necessary for an insulator-to-metal transition. The minimum of the insulating potential well has also shifted causing a coherent motion towards lower x values. The motion is coherent if the pulse width is shorter than the oscillation frequency of the vanadium pairs, which we take to be the experimental value of 6 THz (170 fs).[6,7] The system then enters a period of about 60-80 fs, where n_π barely changes, see Fig. 4. We can identify this period with the structural bottleneck which was observed early on[3]. However, significant changes are occuring in this period. The structural motion initiated by the photoinjection causes a closing of the insulating gap, which can be clearly seen from the changes in electron density around 0 eV in Fig. 5. Although the gap has closed, the system is still in the monoclinic potential well. One also observes a significant relaxation of the electron density in the conduction band due to the electron-electron scattering. After the closing of the gap, the density n_π changes dramatically as electrons start to scatter from the $d_\parallel$ into the d_π bands in order to establish thermal equilibrium. The half period of about 80 fs of the structural oscillation is an important time scale. At this point, the structure, while still monoclinic, ressembles most closely the metallic state. It is also the turning point in the motion and a critical transfer of electrons

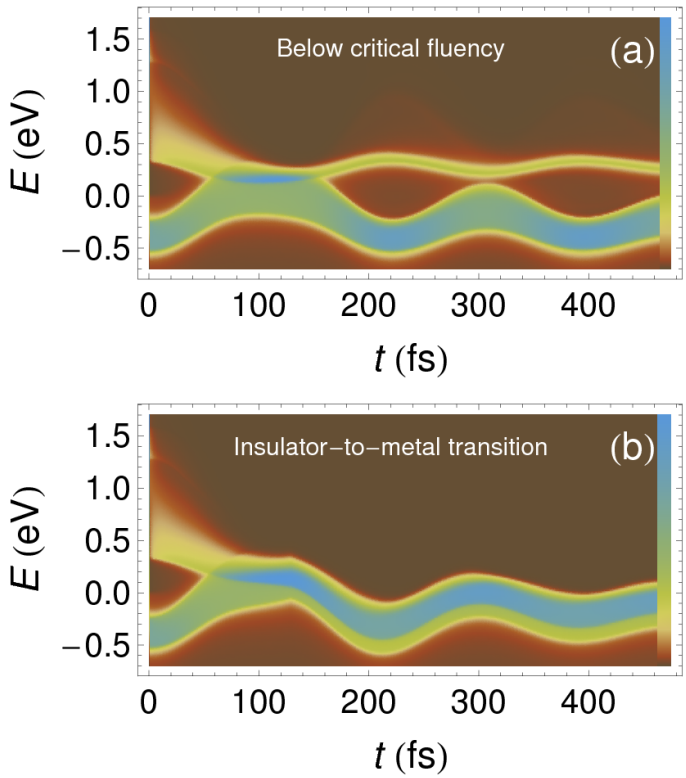

FIG. 5: Total electron densities $n(E,t)$ as a function of energy and time. (a) The total electron density as a function of energy and time for a photoinjected density in the d_π orbital of n_π =0.079, which is below the critical fluency needed for a insulator-to-metal transition. The color scheme accentuates the changes occuring at low electron density, see the scale on the right side. (b) the same but now for n_π =0.086, which is sufficient for an insulator-to-metal transition.

from the $d_\parallel$ into the d_π band needs to occur before the system returns to the insulating monoclinic equilibrium position. As a result of damping of the coherent motion, subsequent periods are less favorable to exchange electrons between the two bands. The increase in electron density strongly depends on the initial photoexcited electron density. If the photoinjected density is below the critical value (here, $n_\pi \leq 0.082$) then the oscillation is not strong enough to allow the critical exchange electrons from the $d_\parallel$ into the d_π states. When the initial electron density exceeds the critical initial density ($n_\pi \geq 0.083$), an avalanche effect occurs. The electron scattering decreases $n_\parallel - n_\pi$ thereby weakening the electrons-lattice coupling, causing a lowering of the metallic minimum, see the dashed lines in Fig. 2. When the system passes the maximum, it rapidly decays into the metallic potential well. The dynamic changes in the energy curve cause a strong deviation from the usual harmonic oscillations in a potential well. After transitioning into the metallic potential well, the system shows a damped oscillatory motion with a frequency of 6 THz. The non-harmonic behavior during the transition period causes a phase shift in the oscillation, see Fig. 4(a). Phase shifts were also seen in terahertz conductivity experiments[6,7], although other effects can also contribute to the phase shift. Very close to the critical initial density n_π=0.082, the system enters an almost stationary monoclinic metallic state from t =100-250 fs. Monoclinic metallic phases have also been observed in microbeams placed on insulating substrates and metallic grids[12].

After the collapse of the insulating band gap, the system can relax in two different ways. If the photoinjected density is below the critical density, the increase in occupation of the d_π band is insufficient to cause an insulator-to-metal transition. The vanadium dimers relax back to their original position and the occupation decreases, see Fig. 4. From Fig. 5(a), we see that the coherent 6-THz oscillations persist, which has also been observed experimentally[6,7]. Although the model includes cooling of the excited electron-hole pairs via coupling with a boson bath at 110 K, we see that the electron density in the d_π band ($n_\pi < 0.1$, see Figs. 4(b) and 5(a)) relaxes slowly and that the system does not return directly to the equilibrium coordinate $x = 1.05$ of the insulating state, see Figs. 4(a). The reason for this slow relaxation is that the scattering of bosons with an energy of the order of 75 meV or less is a rather inefficient way to cool excitations across the insulating gap. This slow relaxation might also explain the presence of a 'hidden' phase in photoinduced manganites[17], which is still insulating but has structural properties that lie between the charge-ordered insulating ground state and the nearly-isotropic metallic phase. When the initial density is higher than the critical density, the system quickly relaxes quickly to the metallic state as soon as it falls into the metallic potential well. Note that the electron densities for energies less than zero and times t >200 fs in 5(a) and (b) are very different. In Fig. 5(a), the low-energy electron density comes from the bonding $d_\parallel$ band and the cut-off is given by the top of the band. The finite electron density for E >0, is the bottom of the d_π band. The chemical potential lies inside the insulating gap. In Fig. 5(b), the electron densities for E <0 consists of the bottoms of both $d_\parallel$ and d_π bands. The cut-off is now given by the chemical potential which lies inside both bands.

The calculated electron densities correspond well to experimentally observed values. For the insulator-to-metal transition throughout the entire film, Cocker *et al.*[10] determined a critical fluency of 15 mJ/cm^{-2}, corresponding to an energy density of around 450 J/cm^3. For a density of 3.3×10^{22} electrons/cm^3, this corresponds to an average energy of approximately 85 meV for each 3d electron. After the Boltzmann scattering has formed a Fermi-Dirac distribution around the gap of 0.5 eV, this corresponds to an excited electron density of around 16%. This is close to the n_π density in the bottleneck period from 10-60 fs in Fig. 4.

The model also explains the absence of metal-to-insulator transitions. Viewing the system as a double-well problem, the transitions between the two states are

expected to be symmetric. To make the transitions unidirectional, an asymmetry in the potential wells[6,7] or the presence of transient states[9] have been suggested. However, a more straightforward explanation is related to the disproportionation of charge between the different orbitals in the insulating state. Photoexcitation affects this imbalance causing a structural motion that leads to the collapse of the insulating gap and a transition into the metallic state. However, in the metallic state, the difference between the charge densities is small. Since the $d_{\|}$ and d_{π} densities of states are very similar in the metallic state, photoexcitation will not create a charge imbalance necessary to induce a coherent motion of the vanadium pairs. Calculations support the idea and show that the electron-hole pair excitations in the metallic state quickly relax to a Fermi-Dirac distribution, followed by subsequent cooling in the absence of any significant structural motion.

IV. CONCLUSIONS

In summary, we have demonstrated that a physically intuitive model combining structural dynamics set into motion by a change in the orbital imbalance necessary to maintain the distortion; a closing of the gap due to the coherent structural motion, followed by electron-electron scattering that drastically changes the potential landscape can explain the photoinduced insulator-to-metal transition in VO_2. The theory also explains many of the key features of the ultrafast phase transition: a structural botteneck of about 80 fs[4], coherent structural motion[6,7] combined with a phase shift in the oscillation[7], the presence of a critical fluency to induce a phase transition[10], and the absence of an ultrafast metal-to-insulator transition. The crucial phase of the transition occurs when the system is metallic while still maintaining the monoclinic structure of the insulating phase[10]. In this transition period, there is a competition between the structural motion trying to return to the insulating monoclinic phase and the electron-electron scattering which tends to drive the system towards electron densities that closely correspond to the metallic state. The ultrafast photoinduced phase transition is nonthermal and cannot be explained by a simple heating of the material. Although we restricted ourselves here to VO_2, the physical picture discussed here is also of relevance for other transition in transition-metal oxides, such as V_2O_3[14], manganites[15–17], and nickelates[21].

Acknowledgments.– This work was supported by the U. S. Department of Energy (DOE), Office of Basic Energy Sciences, Division of Materials Sciences and Engineering under Award No. DE-FG02-03ER46097, the RIXS collaboration as part of the Computational Materials Science and Chemistry Network (CMSCN) under grant DE-FG02-08ER46540, and NIU's Institute for Nanoscience, Engineering, and Technology. Work at Argonne National Laboratory was supported by the U. S. DOE, Office of Science, Office of Basic Energy Sciences, under contract No. DE-AC02-06CH11357.

[1] B. Koopmans, G. Malinowski, F. D. Longa, D. Steiauf, M. Faehnle, T. Roth, M. Cinchetti, M. Aeschlimann, Nature Materials **6**, 259 (2010).

[2] A. Cavalleri, Cs. Tóth, C. W. Siders, J. A. Squier, F. Ráksi, P. Forget, and J. C. Kieffer, Phys. Rev. Lett. **87**, 237401 (2001).

[3] A. Cavalleri, Th. Dekorsky, H. H. W. Chong, J. C. Kieffer, and R. W. Schoenlein, Phys. Rev. B **70**, 161192(R) (2004).

[4] A. Cavalleri, M. Rini, H. H. W. Chong, S. Fourmaux, T. E. Glover, P. A. Heimann , J. C. Kieffer , and R. W. Schoenlein, Phys. Rev. Lett. **95**, 067405 (2005).

[5] D. J. Hilton, R. P. Prasankumar, S. Fourmaux, A. Cavalleri, D. Brassard, M. A. El Khakani, J. C. Kieffer, A. J. Taylor, and R. D. Averitt, Phys. Rev. Lett. **99**, 226401 (2007).

[6] C. Kübler, H. Ehrke, R. Huber, R. Lopez, A. Halabica, R. F. Haglund Jr., and A. Leitenstorfer, Phys. Rev. Lett. **99**, 116401 (2007).

[7] A. Pashkin A. Pashkin1, C. K̈bler, H. Ehrke, R. Lopez, A. Halabica, R. F. Haglund, Jr., R. Huber, and A. Leitenstorfer, Phys. Rev. B **83**, 195120 (2011).

[8] T. Yao, T. Yao, X. Zhang, Z. Sun, S. Liu, Y. Huang, Y. Xie, C. Wu, X. Yuan, W. Zhang, Z. Wu, G. Pan, F. Hu, L. Wu, Q. Liu, and S. Wei, Phys. Rev. Lett. **105**, 226405 (2010).

[9] M. Hada, K. Okimura, and J. Matsuo, Appl. Phys. Lett. **99**, 051903 (2011).

[10] T. L. Cocker, L. V. Titova, S. Fourmaux, G. Holloway, H.-C. Bandulet, D. Brassard, J.-C. Kieffer, M. A. El Khakani, and F. A. Hegmann, Phys. Rev. B **85**, 155120 (2012).

[11] M. Liu, H. Y. Hwang, H. Tao, A. C. Strikwerda, K. Fan, G. Keiser, A. J. Sternbach , K. G. West, S. Kittiwatanakul, J. Lu, S. A. Wolf, F. G. Omenetto, X. Zhang, K. A. Nelson, and R. D. Averitt, Nature **487**, 345 (2012).

[12] Z. S. Tao , T.-R. T. Han, S. D. Mahanti, P. M. Duxbury, F. Yuan, and C.-Y. Ruan, K. Wang, and J. Wu, Phys. Rev. Lett. **109**, 166406 (2012).

[13] K. Shibuya, D. Okuyama, R. Kumai, Y. Yamasaki, H. Nakao, Y. Murakami, Y. Taguchi, T. Arima, M. Kawasaki, and Y. Tokura, Phys. Rev. Lett. **84**, 165108 (2011).

[14] M. K. Liu, B. Pardo, J. Zhang, M. M. Qazilbash, S. J. Yun, Z. Fei, J.-H. Shin, H.-T. Kim, D. N. Basov, and R. D. Averitt, Phys. Rev. Lett. **107**, 066403 (2011).

[15] D. Polli, M. Rini, S. Wall, R. W. Schoenlein, Y. Tomioka, Y. Tokura, G. Cerullo, and A. Cavalleri, Nature Materials **6**, 643 (2007).

[16] P. Beaud, S. L. Johnson, E. Vorobeva, U. Staub, R. A. De Souza, C. J. Milne, Q. X. Jia, and G. Ingold, Phys. Rev. Lett. **103**, 155702 (2009).

[17] H. Ichikawa, H. Ichikawa, S. Nozawa, T. Sato, A. Tomita, K. Ichiyanagi, M. Chollet, L. Guerin, N. Dean, A. Cavalleri, S. Adachi, T. Arima, H. Sawa, Y. Ogimoto, M. Nakamura, R. Tamaki, K. Miyano, and S. Koshihara *et al.* Nature Materials **10**, 101 (2011).

[18] K. W. Kim, A. Pashkin, H. Schafer, M. Beyer, M. Porer, T. Wolf, C. Bernhard, J. Demsar, R. Huber, A. Leitenstorfer, Nature Materials **11**, 497 (2012).

[19] F. Schmitt, P. S. Kirchmann, U. Bovensiepen, R. G. Moore, L. Rettig, M. Krenz, J. -H. Chu, N. Ru, L. Perfetti, D. H. Lu, M. Wolf, I. R. Fisher, Z. -X. Shen, Science **321**, 1649 (2008).

[20] Y. Yusupov, T. Mertelj, V. V. Kabanov, S. Brazovskii, P. Kusar, J.-H. Chu, I. R. Fisher, and D. Mihailovic, Nature Physics **6**, 681 (2010).

[21] W. S. Lee, Y. D. Chuang, R. G. Moore, L. Patthey, M. Trigo, D. H. Lu, P. S. Kirchmann, M. Yi, O. Krupin, M. Langner, N. Huse, J. S. Robinson, Y. Chen, Y . Zhu, S. Y. Zhou, D. A. Reis, R. A. Kaindl, R. W. Schoenlein, D. Doering, P. Denes, W. F. Schlotter, J. J. Turner, S. L. Johnson, M. Forst, T. Sasagawa, Y. F. Kung, A. P. Sorini, A. F. Kemper, B. Moritz, T. P. Devereaux, D.-H. Lee, Z. X. Shen, and Z. Hussain, Nature Comm. **6**, 838 (2012).

[22] K. Yonemitsu and K. Nasu, Physics Reports **465**, 1 (2008).

[23] G. De Filippis, V. Cataudella, E. A. Nowadnick, T. P. Devereaux, A. S. Mishchenko, and N. Nagaosa, Phys. Rev. Lett. **109**, 176402 (2012).

[24] J. B. Goodenough, J. Solid State Chem. **3**, 490 (1971).

[25] S. Biermann, A. Poteryaev, A. I. Lichtenstein, and A. Georges, Phys. Rev. Lett. **94**, 026404 (2005).

[26] L. Whittaker, C. J. Patridge, and S. J. Banerjee, Phys. Chem. Lett. **2**, 745(2011).

[27] J. B. Goodenough, J. Solid State Chem. **3**, 490 (1971).

[28] S. Biermann, A. Poteryaev, A. I. Lichtenstein, and A. Georges, Phys. Rev. Lett. **94**, 026404 (2005).

[29] B. Rethfeld, A. Kaiser, M. Vicanek, and G. Simon, Phys. Rev. B **65**, 214303 (2002).